NANO MICRO small

Carbon Nanotubes

Functionalization of Carbon Nanoparticles Modulates Inflammatory Cell Recruitment and NLRP3 Inflammasome Activation

Marie Yang, Kevin Flavin, Ilona Kopf, Gabor Radics, Claire H. A. Hearnden, Gavin J. McManus, Barry Moran, Adrian Villalta-Cerdas, Luis A. Echegoyen, Silvia Giordani, and Ed C. Lavelle**

The inflammatory effects of carbon nanoparticles (NPs) are highly disputed. Here it is demonstrated that endotoxin-free preparations of raw carbon nanotubes (CNTs) are very limited in their capacity to promote inflammatory responses in vitro, as well as in vivo. Upon purification and selective oxidation of raw CNTs, a higher dispersibility is achieved in physiological solutions, but this process also enhances their inflammatory activity. In synergy with toll-like receptor (TLR) ligands, CNTs promote NLRP3 inflammasome activation and it is shown for the first time that this property extends to spherical carbon nano-onions (CNOs) of 6 nm in size. In contrast, the benzoic acid functionalization of purified CNTs and CNOs leads to significantly attenuated inflammatory properties. This is evidenced by a reduced secretion of the inflammatory cytokine IL-1β, and a pronounced decrease in the recruitment of neutrophils and monocytes following injection into mice. Collectively, these results reveal that the inflammatory properties of carbon NPs are highly dependent on their physicochemical characteristics and crucially, that chemical surface functionalization allows significant moderation of these properties.

1. Introduction

The discovery of carbon nanotubes (CNTs)[1] is regarded as a cornerstone in the advent of nanotechnology. CNTs are nano-sized rolls made of sheets of graphene and are classically coined as single-walled carbon nanotubes (SWCNTs) when they comprise one layer of atoms, while those made of multiple layers are known as multi-walled carbon nanotubes (MWCNTs). The present study focuses on SWCNTs as they were reported to show improved biocompatibility

Dr. M. Yang, Dr. K. Flavin, Dr. I. Kopf, Dr. G. Radics, Dr. S. Giordani,[+]
Dr. E. C Lavelle
Centre for Research on Adaptive Nanostructures and Nanodevices (CRANN)
Trinity College, Dublin 2, Ireland
E-mail: giordans@tcd.ie; lavellee@tcd.ie
Dr. M. Yang, C. H. A. Hearnden, Dr. E. C Lavelle
Adjuvant Research Group
School of Biochemistry and Immunology
Trinity Biomedical Sciences Institute, Trinity College, Dublin 2, Ireland
Dr. K. Flavin, Dr. I. Kopf, Dr. G. Radics, Dr. S. Giordani
School of Chemistry
Trinity Biomedical Sciences Institute
Trinity College Dublin, Dublin 2, Ireland
Dr. G. J. McManus, B. Moran
School of Biochemistry and Immunology
Trinity Biomedical Sciences Institute
Trinity College, Dublin 2, Ireland
Dr. A. Villalta-Cerdas, Prof. L. A. Echegoyen
Department of Chemistry
University of Texas at El Paso
El Paso, Texas, USA
[+]Present address: Italian Institute of Technology, Via Morego 30, 16163 Genova, Italy.

DOI: 10.1002/smll.201300481

and lower cytotoxicity compared to MWCNTs.[2] In addition, SWCNTs represent more homogeneous preparations.[3] While their unique properties have generated tremendous interest in material-based applications, CNTs have also been investigated for biomedical applications including the thermal ablation of tumor cells and drug delivery.[4] The antimicrobial activity and capacity of CNT composites to act as growth scaffolds for bone formation or repair, and neuronal growth have also been reported. Despite encouraging findings, concerns over the toxic and inflammatory properties of CNTs have been raised,[2] particularly in the context of occupational hazards and biomedical applications. Their high aspect ratio (length-to-width) led to concerns that CNTs may cause lung pathologies similar to those caused by asbestos fibres. Authors have attributed a variety of deleterious effects to CNTs: granulomatous inflammation, release of cytosolic enzymes, pulmonary fibrosis, reactive oxygen-induced damage, DNA fragmentation and mitotic spindle disruption (reviewed in [5]). In contrast, other biocompatibility studies have reported no or limited cytotoxicity to macrophages, fibroblasts and osteoblasts,[6–9] and the absence of any tissue damage or inflammation in vivo in mice.[10,11]

These conflicting observations prompted us to revisit the inflammatory potential of carbon nanoparticles, with a particular focus on CNTs and carbon nano-onions (CNOs), a group of carbon allotropes[12–13] that remains underexplored and whose immunomodulatory properties are unknown.

Most studies concerned with the inflammatory properties of CNTs were carried out using "as-prepared" or raw non-functionalized CNTs (*r*-CNTs). However, *r*-CNTs are generally impure as they contain ill-defined amounts of carbonaceous impurities,[14,15] metal catalyst residues[10,16] and microbial contaminants.[17] It is highly probable that such impurities may have contributed to the toxic and immunomodulatory properties previously attributed to CNTs.[18] In the present study, we ruled out the involvement of such impurities by subjecting *r*-CNTs to a rigorous process of purification[19] and ensured that all experiments were carried out in endotoxin-free conditions using medical grade water and ultra pure grade reagents during both synthetic, in vitro and in vivo work.[20] CNTs possess the inherent tendency to form aggregates in both aqueous and organic solvents and this can be addressed by means of surface functionalization. We recently reported the purification and selective oxidation of CNTs (*p*-CNT) while minimizing the effects of the chemical treatment on their integrity or shape,[19] however the consequence of this on their inflammatory properties was not investigated.

Insoluble aluminium salts—generically referred to as alum[21]—have served as particulate immunopotentiators in vaccines for over 80 years and millions of doses of alum-containing vaccines have been administered to healthy patients. A large body of evidence showed that alum exerts cytotoxic and inflammatory effects both in vitro and in vivo,[22] however, these effects are clearly acceptable given the excellent record of alum as a clinically applied vaccine adjuvant. Here, the immunomodulatory properties of CNTs and CNOs were compared to those of alum. In recent years, the NLRP3 inflammasome has been implicated in the inflammatory properties of particulate materials, including those of alum. Along with the adaptor protein ASC (apoptotic speck protein containing a caspase recruitment domain) and procaspase-1, NLRP3 forms a molecular platform responsible for the catalytic activation of caspase-1, and the cleavage and release of the inflammatory cytokines IL-1β and IL-18.[23] Previous studies have described NLRP3 inflammasome activation by raw non-functionalized multi-walled CNTs.[24,25] Here, in the context of their potential biomedical applications, we present a comprehensive analysis of the inflammatory and NLRP3 inflammasome activation properties of raw, purified and functionalized single-walled CNTs and small CNOs. We show that these properties are dependent on the physicochemical characteristics of the carbon allotrope and importantly that surface functionalization represents a convenient and controlled means to temper these inflammatory attributes.

2. Results

2.1. Preparation and Characterization of Carbon Nanotubes and Nano-Onions

r-CNTs were purified following a novel and recently described procedure,[19] (**Figure 1**A), which allows for the preparation of high purity *p*-CNT, where both carbonaceous impurities and iron catalyst are removed with high efficiency. This procedure takes advantage of a short nitric acid oxidation treatment to reduce structural/electronic degradation of the CNTs and sodium hydroxide treatments to remove carboxylated carbonaceous impurities. Essential to the purification, however, is the second oxidation step with hydrogen peroxide, which facilitates decomposition of the remaining carbonaceous impurities and full conversion of oxygenated groups to carboxylic acid functionalities (Figure 1A). AFM analysis of *r*-CNTs vs *p*-CNT was carried out to confirm the purity of the samples used in the study (Supporting Information Figure S1). Size distribution analysis of *p*-CNT revealed an average length ranging from 128 to 445 nm and an average diameter of 0.7 to 1 nm (Supporting Information Figure S2). The CNOs used in the study were synthesized according to a previously described procedure by annealing of nanodiamonds[26] which leads to highly pure materials with homogeneous diameters of 5-7 nm (Figure 1 and Supporting Information Figure S2).

Both *p*-CNT and *p*-CNO were subsequently functionalized to produce *f*-CNT (Figure 1A) and *f*-CNO (Figure 1B), using a previously described[27–29] one-pot Tour reaction comprising aminobenzoic acid and isoamylnitrite. This reaction was chosen because of its simplicity, versatility and the fact that its chemistry occurs at the sidewall of the carbon NPs. Evidence of the covalent modification is provided in Supporting Information Figure S3, with spectra showing a substantial enhancement of the D-band (activated by the presence of defects on the carbon NPs following the chemical treatment). FTIR analysis of the samples following the chemical treatment shows the appearance of aromatic C-H deformation vibrations (1290–990 cm^{-1}), aromatic C = C (1600 and 1475 cm^{-1}) and C-O (≈1625 and ≈1725 cm^{-1}) stretching vibrations, and O-H vibrations (1300 cm^{-1}). While the Zeta potential of –33.8mV for *p*-CNT indicates an increase in

small 2013,
DOI: 10.1002/smll.201300481

NANO MICRO small

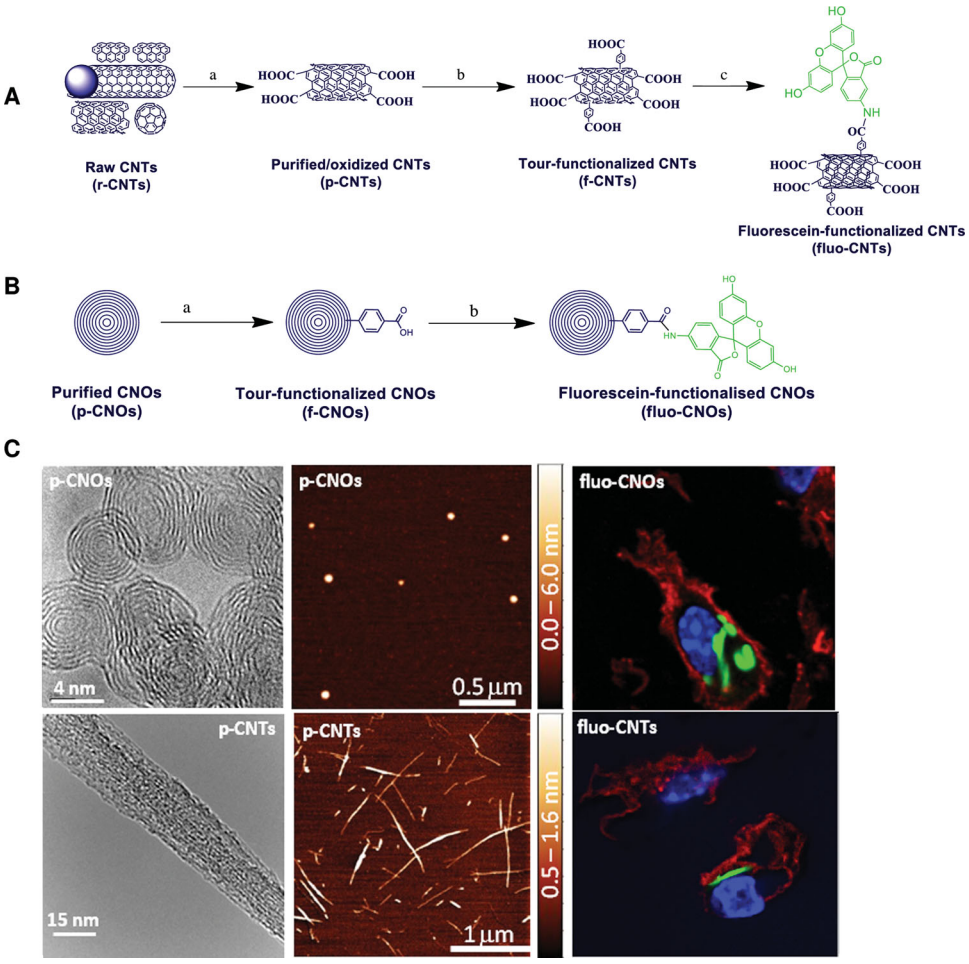

Figure 1. Schematic of carbon nanoparticle purification and functionalization. A) CNT purification and functionalization protocol. a) 7.9 M HNO_3, 100 °C, 4.5 h; 2 M NaOH, 100 °C, 12h (2×); 10% H_2O_2, 100 °C, 1 h; 2% H_2O_2, 20 °C, 12 h; 2 M NaOH, 100 °C, 12 h. b) 4-aminobenzoic acid, isoamyl nitrite, NMP, 70 °C, 14 h, N_2. c) DMAP, N-hydroxysuccinimide, DMF, 10 min; EDCI, 3 h, N_2; Fluoresceinamine, 60 °C, 6 days, N_2. B) CNO functionalization protocol. a) aminobenzoic acid, isoamyl nitrite, DMF, N2, 60 °C, 16 h; b) DMAP, N-hydroxysuccinimide, DMF, 10 min; EDCI, 3 h, N_2; Fluoresceinamine, 60 °C, 6 days, N_2. C) Visualization of carbon nanoparticles. High resolution TEM images of p-CNOs and p-CNTs nanoparticles (left panels). AFM topographs of p-CNO and p-CNT deposited on mica (middle panels). Confocal microscopy of C57BL/6 BMDCs incubated in the presence of fluorescein (green) labelled -CNT and -CNO for 18 h, then washed in PBS, fixed, and stained with wheat germ agglutinin-Alexa Fluor594 (red) and nuclei stain Hoescht (blue) (right panels).

polarity relative to *r*-CNT (–23.7 mV) (Supporting Information Figure S5, B), the further lowering in the Zeta potential to –38.7 mV for *f*-CNT and to –16.8 mV for *f*-CNO at pH 7.3 is in agreement with the successful surface functionalization.

To allow for in vitro visualization of the functionalized particles, a standard amide coupling reaction was used to covalently attach fluoresceinamine, thus producing *fluo*-CNTs and *fluo*-CNOs (Figure 1). The absorption and emission spectra of fluorescein-functionalized materials are represented in Supporting Information Figure S4. To minimize contamination of all purified and functionalized materials by microbial contaminants, such as endotoxins, samples were dispersed in NMP by water bath sonication (80 kHz), dialyzed against medical grade sterile water for 5 days and lyophilized until dry in sterile glass containers.

During functionalization, the size of individual CNPs does not change significantly as evidenced by AFM measurements. The agglomeration tendency changes are shown by DLS measurements performed in saline buffer, which was used as the particle suspension vehicle for the immunological studies. The initial particle sizes for *f*-CNOs and fluo-CNOs were 170 ± 11 nm and 136 ± 9 nm, respectively, after sonication and the agglomeration curve as a function of time is represented in Figure S5. Unlike the round CNO particles, CNTs are rod like structures with high aspect ratios and angle dependent light scattering, and are characterized by their effective hydrodynamic diameter in single angle light scattering.[30] Following the same sample preparation and measurement conditions as above, CNTs showed multimodal distribution of particle sizes in all cases (Supporting Information Figure S5C).

2.2. Dendritic Cells and Macrophages Take up Carbon NPs

We sought to evaluate the ability of macrophages (Macs) and dendritic cells (DCs) to internalize single-walled CNTs

DOI: 10.1002/smll.201300481

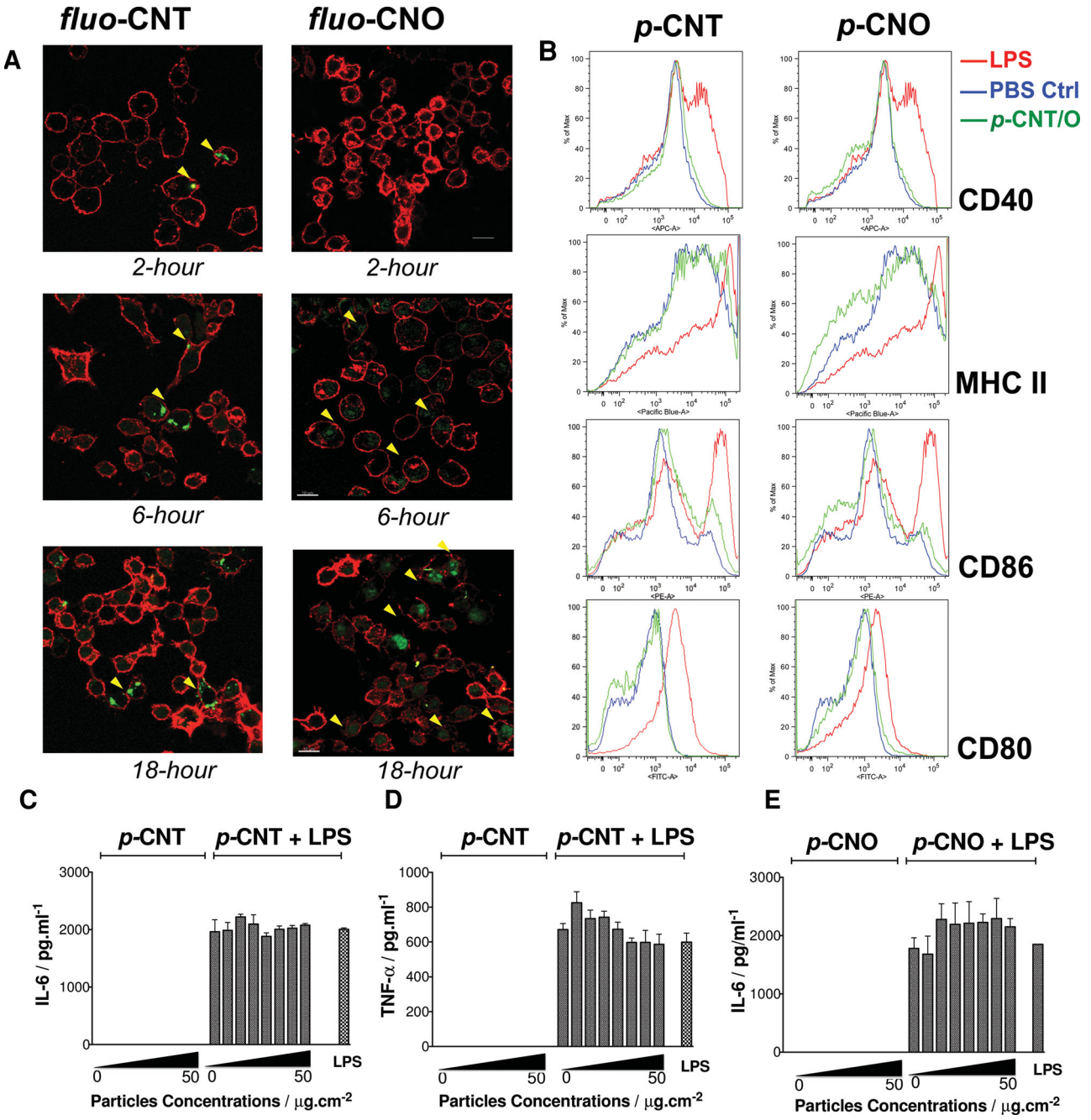

Figure 2. CNTs and CNOs are efficiently taken up by antigen-presenting cells, but do not induce maturation of dendritic cells nor production of inflammatory cytokines. A) Confocal microscopy of wild-type iBMM incubated in the presence of fluorescein (green) labelled-CNT and -CNO for 2, 6, and 18 h, then washed in PBS, fixed, and stained with wheat germ agglutinin-Alexa Fluor594 (red). Original magnification, ×60. B) The expression of the maturation markers CD40, CD80, CD86 and MHCII (I-A/I-E) was measured by flow cytometric analysis in BMDC cultures treated with either alum, p-CNT or p-CNO at 50 µg cm^{-2} for 24 h. C,E) Quantification of IL-6 (C,E) and TNF-α (D) in supernatants of BMDC cultures incubated for 24 h with p-CNT ± 1 ng mL^{-1} of LPS or p-CNO ± 1 ng mL^{-1} of LPS at concentrations ranging from 0.4–50 µg cm^{-2}.

and small CNOs, using confocal microscopy. Immortalized bone-marrow derived mouse macrophages (iBMM) were incubated in the presence of fluorescein-labeled CNTs (*fluo*-CNTs) and small CNOs (*fluo*-CNOs) over a time course of 18 h (**Figure 2**A). Results indicate that the internalization of *fluo*-CNOs by iBMM occurs to a higher degree compared to *fluo*-CNTs, as indicated by a greater number of green patches (yellow arrowheads), particularly at 6 and 18 h. Similarly, confocal imaging of mouse bone-marrow-derived dendritic cells (BMDCs) revealed the uptake of carbon NPs (Supporting Information Figure S6), although to a lesser extent than in Macs. This is not surprising as Macs are known to exhibit higher phagocytic activity than DCs.[31]

Live imaging of iBMMs incubated in the presence of *p*-CNT and *p*-CNO (50 µg cm^{-2}) shows that dendrites are being formed within 30 min of incubation indicating that

small 2013,
DOI: 10.1002/smll.201300481

NANO MICRO small

carbon NPs are being actively sensed by professional antigen-presenting cells (Supporting Information Movies 1–3). Previous studies have documented the ability of CNTs to induce activation and maturation of DCs,[32,33] while others reported contradictory findings.[34–35] These conflicting results prompted us to assess the expression of surface markers CD40, CD80, CD86 and MHC class II (I-A/I-E) in BMDC cultures treated with either alum or highly purified *p*-CNT or *p*-CNO at a range of concentrations (Figure 2B). There was no distinguishable effect on expression of any of these cell surface markers when compared to their respective controls (Figure 2B). Studies have also described that commercial preparations of carbon nanotubes could induce the production of the cytokines IL-6, TNF-α and IL-1β by RAW 264.7 macrophages[36] as well as systemically (plasma) in vivo,[37] however, most of these studies fail to report endotoxin content. Our study indicates in contrast that neither *p*-CNTs nor *p*-CNOs induce secretion of the inflammatory cytokines IL-6 or TNF-α and did not significantly alter LPS-induced secretion of these two inflammatory cytokines (Figure 2 C–E). Using the LAL Chromogenic Endotoxin quantification kit (Pierce), we found that in correlation with the IL-6 readout from BMDCs cultures, the absorbance values for all the CNT and CNO preparations used in these studies were not greater than those of the negative control, endotoxin-free water (Supporting Information Figure S7). Likewise, we also demonstrated that CNTs and CNOs induced negligible death in BMDC cultures (Supporting Information Figure S8).

2.3. Purified Carbon NPs Promote Secretion of IL-1β in a NLRP3- and Dose-Dependent Manner

The particulate nature of CNTs and CNOs prompted us to investigate their ability to promote the secretion of IL-1β and the involvement of the NLRP3 inflammasome. BMDCs stimulated with LPS (1 ng mL^{-1}) alone or *p*-CNT alone secreted low or undetectable amounts of IL-1β, while stimulation of LPS-primed cells from C57BL/6 mice with *p*-CNT alone resulted in significantly enhanced secretion of IL-1β (**p = 0.0014, **Figure 3**A) in a dose-dependent manner. Most interestingly, we show for the first time that, similarly to *p*-CNT, small *p*-CNOs can induce the release of IL-1β by DC upon TLR-ligand priming (* p = 0.022, Figure 3B), albeit to a lesser extent than p-CNTs. Indeed, at concentrations ranging from 0.35–50 μg.mL^{-1}, small *p*-CNOs were 2-5 times less potent than *p*-CNTs at inducing the secretion of IL-1β (**p = 0.0012). Importantly, these effects were not restricted to priming with LPS (a TLR4 agonist), as a synergistic IL-1β production was also obtained upon priming with the TLR2 agonist Pam3CSK4 and the TLR9 agonist CpG (Supporting Information Figure S9).

Previously, Yazdi et al.[38] reported that CNTs failed to induce activation of the NLRP3 inflammasome in bone-marrow derived macrophages in contrast to two other studies which found that raw non-functionalized multi-walled CNTs could induce its activation. These latter investigations were carried out on human primary macrophages or monocytes using siRNA-based approaches.[24,25] Here, we show that the secretion of IL-1β in response to LPS plus alum, *p*-CNT or *p*-CNO was abolished in BMDCs generated from $NLRP3^{-/-}$ mice (Figure 3C,D). To confirm that this effect on IL-1β secretion was not reflective of a generalized hyporesponsiveness of $NLRP3^{-/-}$ cells, we assayed the same supernatants for IL-6, whose production occurs independently of caspase-1 activation.[39] IL-6 was secreted at comparable level in cells stimulated with LPS alone or LPS plus *p*-CNT/*p*-CNO in both wild type and $NLRP3^{-/-}$ cells (Supporting Information Figure S10). In order to provide more direct evidence that both CNTs and CNOs induce activation of the NLRP3 inflammasome, we tested their ability to induce oligomerization of ASC which is essential for full activation of the NLRP3 inflammasome.[40] We thus performed confocal imaging of THP-1 cells stably transfected with ASC-GFP (ASC-GFP-THP-1 cells) and visualized the cells by confocal microscopy (Figure 3E). No or very few ASC-GFP specks were observed when ASC-GFP-THP-1 cells were treated with PBS, LPS alone or *p*-CNT alone. On the other hand, when cells were pulsed with LPS and incubated in the presence of *p*-CNT, multiple and larger green specks were visible (Figure 3E, yellow arrows). Addition of the cathepsin B inhibitor Ca-074-Me to BMDC cultures primed with LPS resulted in an impaired production of IL-1β (Figure 3F), suggesting that lysosomal damage and release of cathepsin B is essential for carbon particle-induced NLRP3 inflammasome activation.[41,42] The involvement of caspase-1 was determined by the use of the caspase-1 inhibitory peptide YVAD-fmk, which led to a significant decrease of IL-1β secretion (Figure 3F). Finally, we also showed that lysosomal acidification and potassium efflux were required for inflammasome activation by carbon NPs (Supporting Information Figure S11).

2.4. Chemical Functionalization of Carbon NPs Attenuates Their Inflammatory Properties in Vitro and in Vivo

Having shown that *p*-CNT and *p*-CNO could activate the NLRP3 inflammasome in the presence of TLR ligands, we investigated whether chemical functionalization could modulate these inflammatory properties. Incubation of LPS-primed BMDCs in the presence of *p*-CNT resulted in significantly greater production of IL-1β compared to incubation with *raw*-CNT, while in contrast, IL-1β production by cells incubated with *f*-CNT was significantly lower than with *r*-CNT (**Figure 4**A, ***p < 0.001, r-CNT *vs.* *p*-CNT and *f*-CNT at concentrations of 6-50 μg cm^{-2}). Similarly, the benzoic acid-functionalization of *p*-CNOs led to a significant reduction in particle-induced secretion of IL-1β (Figure 4B, * p< 0.05, p-CNO vs *f*-CNO at concentrations of 3–50 μg cm^{-2}). For both CNTs and CNOs, benzoic acid-functionalization led to an enhanced dispersibility in both organic and aqueous diluents, a difference that remained visible up to 24 h after sonication (as shown for CNOs, Figure 4C). Another noteworthy observation was that CNOs were less inflammatory than CNTs, regardless of their functionalization status.

To further understand the modulatory properties of carbon NPs on innate immune responses, we carried out studies using a mouse peritonitis model. C57BL/6 mice

DOI: 10.1002/smll.201300481

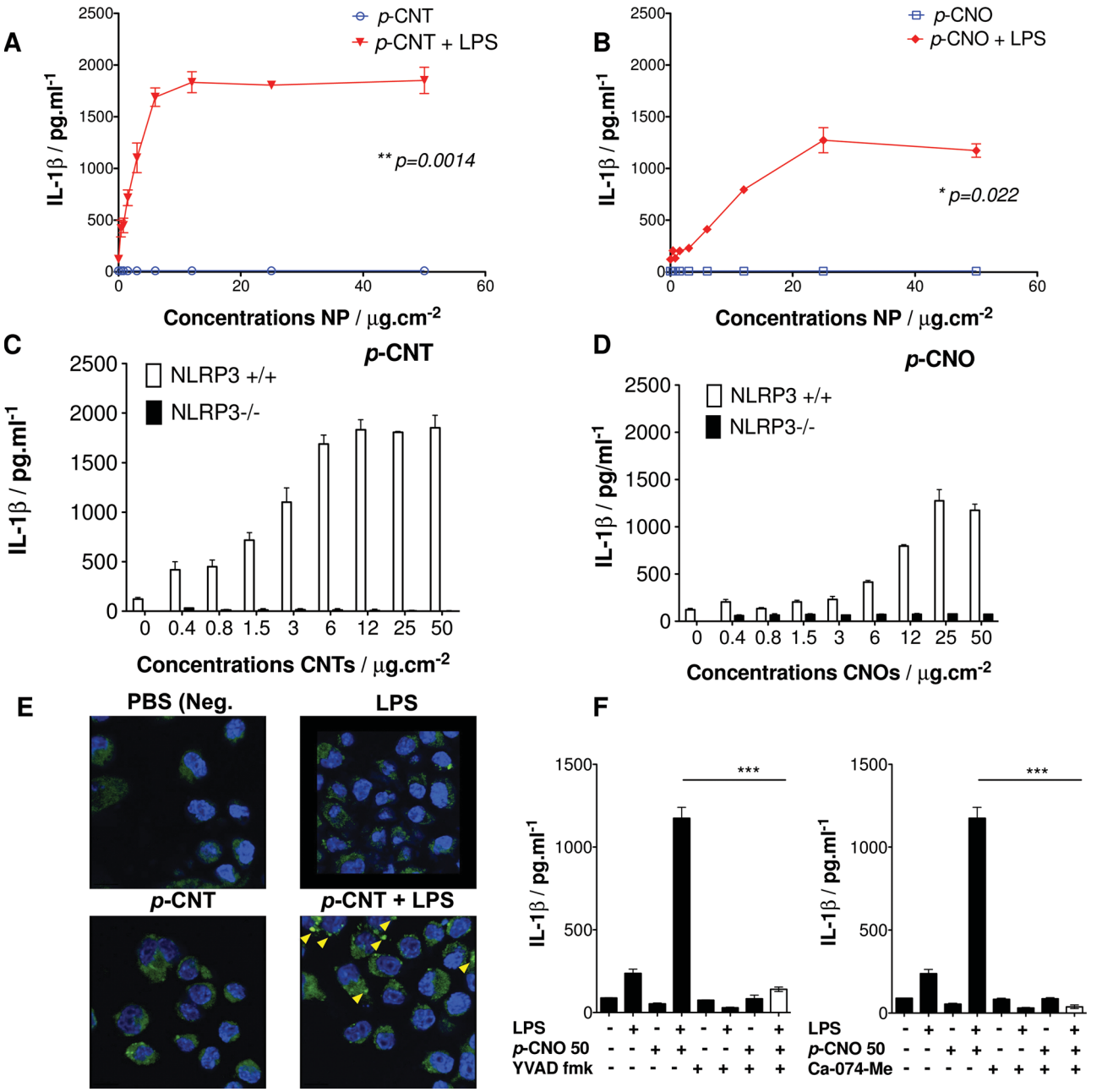

Figure 3. CNTs and CNOs induce the synergistic secretion of IL-1β in a NLRP3-dependent manner. A) Carbon nanotubes and B) nano-onions (dose range: 0.4–50 μg cm^{-2}) were added to C57BL/6 BMDC cultures either alone or in combination with LPS (1 ng mL^{-1}). Supernatants were collected after 24 h incubation and assayed by ELISA (*p* = CNO vs *f*-CNO t-test; *r*-CNT vs *p*-CNT or *f*-CNT (ANOVA and Dunnett's post hoc test, *p < 0.05, *** p< 0.001). C) Carbon nanotubes and D) nano-onions (dose range: 0.4–50 μg cm^{-2}) were added to either C57BL/6 or $NLRP3^{-/-}$ BMDC cultures either alone or in combination with LPS (1 ng mL^{-1}). Supernatants were collected after 24 h incubation and assayed by ELISA. E, ASC-GFP THP-1 cells were left untreated (PBS), treated with LPS (1 μg mL^{-1}) or treated with LPS +/– p-CNT (25 μg cm^{-2}) for 6 h and observed by confocal fluorescence microscopy (Original magnification: 40×). F, ELISA for IL-1β. Resting or LPS-primed BMDCs were stimulated with p-CNO (25 μg cm^{-2}) in the absence or presence of the cathepsin B inhibitor Ca-074-Me (10 μM) or the caspase-1 inhibitor YVAD-fmk (***p < 0.001, *p*-CNO+LPS *vs.* *p*-CNO+LPS+ chemical inhibitor).

were administered with PBS vehicle suspensions containing alum, *r*-CNT, *p*-CNT, *f*-CNT, *p*-CNO or *f*-CNO. The nature of the infiltrating cells recruited into the peritoneal cavity was determined using flow cytometry at 3 h post-injection (**Figure 5**). $CD11b^{+}F4/80^{+}$ macrophages are one of the most prominent resident cell populations in the mouse peritoneum. Here, in line with previous reports,[43,44] we observed a dramatic reduction (from 29.6% to 3.4%) in the number of $CD11b^{+}F4/80^{+}$ expressing cells when mice were injected with alum (Figure 5, top panel). We show for the first time that injection of CNT or CNO also results in a depletion of resident peritoneal macrophages. Specifically, depletion of resident macrophages occurred in mice administered with *p*-CNT (from 29.6% to 4.13%), *f*-CNT (from 29.6% to 12.6%),

small 2013,
DOI: 10.1002/smll.201300481

small NANO MICRO

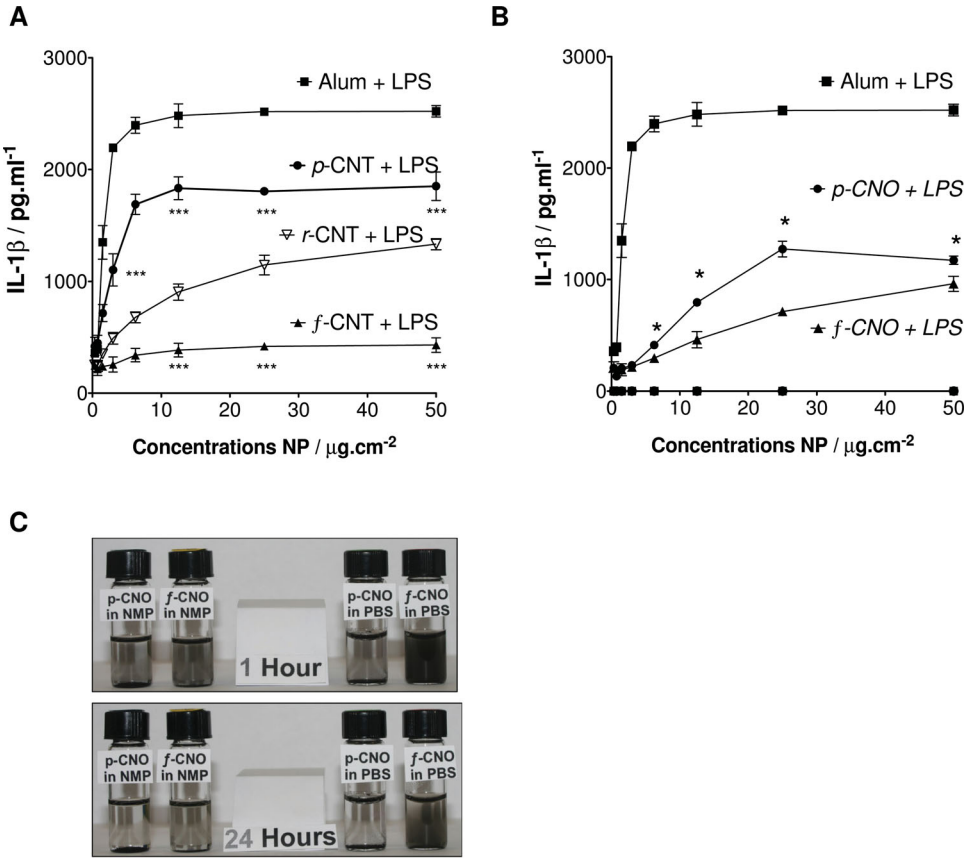

Figure 4. Tour-functionalization of *p*-CNOs and *p*-CNTs attenuates their inflammatory properties in vitro. A,B) Raw *r*-CNTs, *p*-CNT, *p*-CNO, *f*-CNT or *f*-CNO (dose range: 0.25–50 μg cm^{-2}) were added to C57BL/6 BMDC cultures in combination with LPS (1 ng mL^{-1}) or with LPS alone. Supernatants were collected after 24 h incubation and cytokines were assayed by ELISA (*p* = CNO vs *f*-CNO t-test; *r*-CNT vs. *p*-CNT or *f*-CNT ANOVA and Dunnett's *post hoc* test, ∗ $p < 0.05$, ∗∗∗$p < 0.001$). C) Photograph showing increased dispersibility of *p*-CNOs and *f*-CNOs in organic (NMP) and aqueous (PBS) solvents upon Tour-functionalization at 1 and 24 h after sonication.

p-CNO (from 29.6% to 16.8%) and *f*-CNO (from 29.6% to 20.5%) preparations (∗∗∗$p < 0.001$, Dunn's post hoc test) in comparison to PBS control group). Remarkably, no significant changes were observed in mice injected with *r*-CNT (from 29.5% to 25.7%) (Figure 5, top panel). In contrast to the depletion of resident macrophages, a marked recruitment of $Ly6G^{+}SiglecF^{-}$ neutrophils and $CD11c^{-}Ly6C^{High}$ inflammatory monocytes—described in the literature as potential DC precursors[44]—was detected in mice administered with *p*-CNT, *f*-CNT, *p*-CNO and *f*-CNO, as well as in the alum group (Figure 5B,C). Here again, there was no significant neutrophil or monocyte recruitment in the *r*-CNT group in comparison to the PBS group. Within each subset of carbon NPs, the benzoic acid-functionalized particles were consistently 2-5 times less effective than their purified counterparts at recruiting inflammatory cells (Histograms, ∗$p < 0.05$ and ∗∗$p < 0.01$, Dunn's post hoc test, Figure 5B). Most interestingly, and in line with the in vitro results presented earlier, CNOs were consistently less potent than CNTs at inducing either resident macrophage depletion or neutrophil and monocyte recruitment (∗$p < 0.05$, two-tailed t-test).

In view of these results on the regulation of innate immunity by carbon nanoparticles, we then assessed the potential of purified and functionalized carbon NPs to modulate adaptive immune responses. An adjuvant study was carried out to assess whether co-administration of carbon NPs with human serum albumin (HSA) in mice can enhance antigen specific cellular or humoral immunity. In contrast to the established vaccine adjuvant alum, none of the carbon NPs preparations tested induced a significant increase in specific antibody responses (HSA-specific IgG and IgG1) (Supporting Information Figure S12A). Instead, we found that carbon NPs, and CNOs in particular, promoted secretion of the immunosuppressive cytokine IL-10 in mediastinal lymph node cultures (Supporting Information Figure S12B, ∗∗∗$p < 0.001$, Dunnett's test individual group vs HSA group).

3. Discussion

The current lack of consensus on the inflammatory properties of carbon NPs represents a significant issue regarding their application in the biomedical field. Here we explored the ability of carbon nanotubes and nano-onions to promote inflammation, how this relates to their physicochemical properties and the use of surface functionalization to modulate their inflammatory properties.

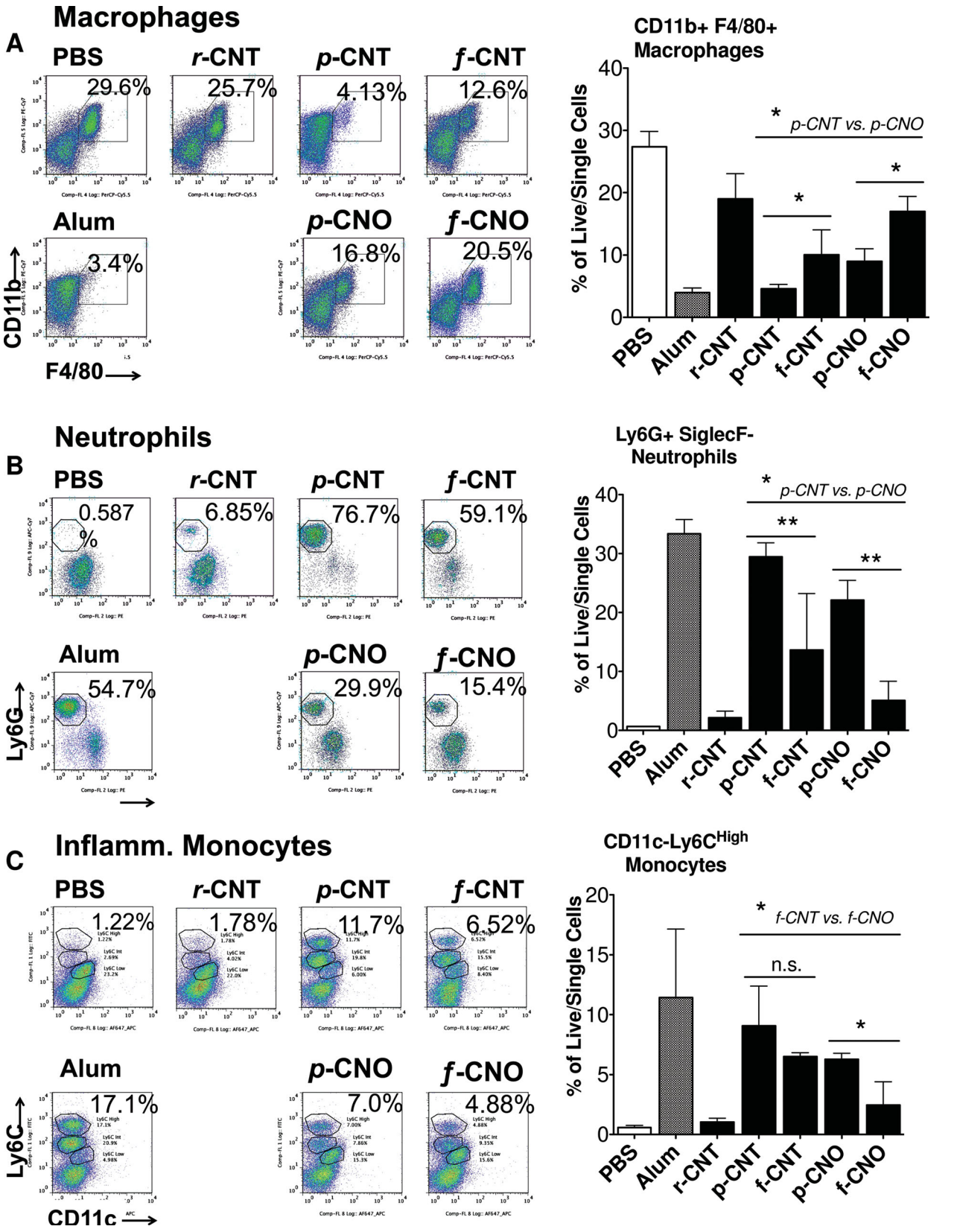

Figure 5. Tour-functionalization modulates the inflammatory properties of CNTs and CNOs in vivo. A–C) Female C57BL/6 mice (n = 3–5) aged 6–8 weeks were injected intraperitoneally with PBS vehicle, Alum (250 μg/mouse), r-CNTs (250 μg/mouse), *p*-CNT (250 μg/mouse), *f*-CNT (250 μg/mouse), *p*-CNO (250 μg/mouse) or *f*-CNO (250 μg/mouse). After 3 hr, peritoneal lavage cells were collected and cell recruitment was analysed by flow cytometry. The combinations of markers used to characterize the peritoneal cell recruitment were defined as follows: A) $CD11b^{High}$ F4/80+ macrophages, (B $Ly6G^{+}$ Siglec F^{-} neutrophils, and C) $CD11c^{-}Ly6C^{High}$ inflammatory monocytes. Results are expressed as a percentage of single/live cells (* $p < 0.05$, ** $p < 0.01$, Dunn's post hoc test).

small 2013,
DOI: 10.1002/smll.201300481

NANO MICRO small

Firstly, we established that highly purified preparations of CNTs and CNOs fail to induce dendritic cell maturation (Figure 2B) or to stimulate any detectable level of inflammatory cytokine secretion (Figure 2C–E) in vitro. These results are in line with Brewer et al.,[45] who demonstrated that particulate materials, including commercial vaccine adjuvants such as alum salts, are unable to act as TLR agonists and do not induce DC maturation.[46] The results are, however, in contrast to earlier reports which documented the inflammatory potential of commercial CNTs[33] and their ability to induce DC maturation and secretion of cytokines such as IL-6 and TNF-α.[47,48] It is possible that in these reports, the *raw* preparations tested may have contained immunostimulatory contaminants[17,49] although differences in assay systems and cell types may also contribute to the differences observed.

Secondly, we describe for the first time, as anticipated by their particulate nature,[50] that not only single-walled CNTs but also small CNOs promote secretion of the proinflammatory cytokine IL-1β by BMDC in a NLRP3- and dose-dependent manner, in the presence of TLR ligands (Figure 3). An earlier study reported that large CNOs (30 nm diameter) were 10 times less cytotoxic than multi-walled CNTs using a human skin fibroblast cell line.[51] Here, we found that small CNOs exhibit an inflammatory profile that is weaker than that of single-walled CNTs both in vitro with respect to the release of IL-1β by BMDCs (Figure 4, $^{**}p < 0.01$, not shown) and in vivo with respect to the recruitment of neutrophils and inflammatory monocytes (Figure 5, $^{*}p < 0.05$). It is highly probable that the long fiber-like morphology of CNTs *vs.* the spherical shape and minute size[26] of CNOs may contribute to these differences. We determined that CNOs were taken up by antigen-presenting cells (Figure 1A,B and Supporting Information S6) to a greater extent than CNTs. However, CNOs were less competent at inducing NLRP3 inflammasome activation and secretion of IL-1β, suggesting that the magnitude of the response is not strictly proportional to particle uptake. Similarly, we found that in vivo CNOs were more efficiently targeted to draining lymph nodes (Supporting Information Figure S13A) when compared to single walled-CNTs. This finding was supported by raman spectral analysis (Supporting Information Figure S7B). Overall, by virtue of their weak inflammatory potential and low cytotoxicity (Supporting Information Figure S9), yet efficient uptake by antigen-presenting cells and transport to lymph nodes, CNOs may represent a safer and more efficient alternative to CNTs for applications such as drug delivery[52] or in biocomposite materials.[53]

Thirdly, we assessed the impact of surface functionalization on the inflammatory response to carbon nanoparticles.[54] In striking contrast to the relative immunological inertia of *r*-CNTs, purified *p*-CNTs and *p*-CNOs were highly potent at recruiting innate cells including neutrophils and monocytes (Figure 5). Remarkably however, the benzoic acid-functionalization of both purified carbon NPs resulted in a significantly reduced inflammation in vitro with regard to the release of IL-1β (Figure 4) as well as in vivo with regard to the recruitment of innate inflammatory cells (Figure 5). To our knowledge, this study is the first to describe the potential for selective oxidation and surface chemical functionalization to exert fine control over the inflammatory properties of carbon nanoparticles.

We sought to comprehend the basis for the differential inflammatory abilities of *r*-CNTs vs. *p*-CNT vs. *f*-CNT as well as *p*-CNOs vs. f-CNOs, and therefore carried out detailed studies on particle agglomeration, size and polarity. The zeta potential of carbon particles was determined and can be categorized as follows: *r*-CNTs>*p*-CNT*s*>*f*-CNTs and *p*-CNOs>*f*-CNOs (Supporting Information Figure S5). A decreasing zeta potential denotes an increased polarity, which correlates well with the enhanced dispersibility in aqueous solvents[19] and is evidenced in Figure 4 (photograph). The contrasting inflammatory effects of CNTs and CNOs may reflect differences in size but these particles also differ in other physical characteristics including shape. A size-dependent effect has indeed been described in previous studies investigating the inflammatory profile of particulate materials,[55,56] which found that larger particles are generally less inflammatory than their smaller counterparts. While strong hydrophobic forces are known to induce spontaneous and rapid agglomeration in *r*-CNTs, it is reasonable to suggest that an increased polarity in *p*-CNTs may have hampered this agglomeration leading to the formation of smaller sized-aggregates over the same period of time and hence the enhanced inflammatory responses induced by *p*-CNTs than *r*-CNTs. However, further lowering of zeta potential in *f*-CNTs as a result of benzoic acid functionalization resulted in a decreased inflammatory potential compared with *p*-CNT (Figures 4 and 5). Therefore, despite the enhanced dispersibility of *f*-CNTs (and *f*-CNOs), their inherent polarity led to a reduced local inflammatory response.

4. Conclusion

Our study suggests that the inflammatory properties of carbon NPs, in particular CNTs, may have been overestimated in the current literature and importantly, that simple and carefully designed functionalization strategies may allow for tight control of carbon NP-induced inflammation. Specifically we found that raw CNT induced very limited inflammation in vitro or in vivo while purified CNT induced marked inflammasome activation in vitro and inflammatory responses in vivo which were significantly attenuated by benzoic acid functionalization. We further show that CNO promote less inflammation than carbon nanotubes and this can be further reduced by surface functionalization.

5. Experimental Section

Preparation of Carbon Nanotubes and Nano-Onions for in Vitro and in Vivo Studies: Raw single walled carbon nanotubes (*r*-CNTs) produced by the HiPco technique were purchased from Unidym, Inc. (Lot no R0513). Reagents and solvents used for the purification and chemical functionalization of carbon NPs were purchased as reagent-grade from Fisher Scientific Ireland Ltd, or Sigma-Aldrich Ireland and used without further purification.

Highly Purified Selectively Oxidized CNTs (p-CNTs): Synthesis was performed as previously described.[19] A 300 mg quantity of raw SWNTs was dispersed in 7.9 M HNO_3 (1000 mL) by sonication

DOI: 10.1002/smll.201300481

(sonic waterbath, at 80 kHz) at maximum power for 5 min and subsequently at minimum power for 10 min. The mixture was then stirred under reflux at 100 °C for 4.5 h and quenched with ice. The dispersion was then filtered through a Millipore system (0.2 μm Isopore filter) and washed with distilled water until the filtrate ran neutral. The wet solid was transferred to a Teflon tube, dispersed in 2 M NaOH by sonication for 5 min and subsequently stirred overnight at 100 °C under a nitrogen atmosphere. The mixture was cooled to room temperature, filtered through an Isopore filter and washed with a further 500 mL of 2 M NaOH. The solid was washed with distilled water until the filtrate pH became neutral and the sample was subjected to the NaOH treatment one additional time. Following filtration, the wet solid was dispersed in 10% H_2O_2 by sonication for 5 min and subsequently stirred for 1 h at 100 °C. The dispersion was quenched with ice (800 g, diluting to 2% H_2O_2) and allowed to stand for 12 h. The wet solid was subsequently subjected to two further NaOH treatments (as above), and filtered. The solid was then washed with 2 M NaOH (400mL), followed by distilled water until neutral pH, and a further 1 M HCl (400 mL), followed by distilled water until neutral pH. The wet solid was re-dispersed in distilled water and lyophilized to afford 51 mg of black solid (yield: 17%). A portion of this material was dialyzed (10–13 kDa CO) against medical grade (endotoxin free) sterile water (Baxter) for 5 days. The 5-day dialysis entailed two daily changes of water preceded by a 60- to 90-min sonication at 80 kHz. At the end of the dialysis period, all preparations were placed in sterile glass containers and lyophilized until dry.

Pristine CNOs (p-CNOs): Synthesis was performed by annealing of nanodiamonds as previously described.[26] Briefly, high purity ultradispersed nanodiamonds (Molto Ig, Inc.) were annealed in a graphite crucible at 1650 °C in an Astro carbonization furnace under a partial pressure of helium (approx. 150mm). The temperature was maintained for 1 hr and the sample was cooled to RT over a period of 1 h. This procedure was followed by annealing of the sample in air at 400 °C to remove amorphous carbon and the recovered material was composed mainly of pristine CNOs, 95% recovered mass.

Tour-functionalized CNTs (f-CNTs): Synthesis was performed according to a procedure previously described.[27] A 45 mg quantity of *p*-CNTs was dispersed in N-Methyl-2-pyrrolidone (NMP, 200 mL) by sonication for 20 min. Following addition of 4-aminobenzoic acid (1.1g), the reaction mixture was put under a nitrogen atmosphere. The reaction mixture was stirred overnight at 70 °C, following addition of isoamyl nitrite (1.6 mL) *via* syringe. After cooling to room temperature, the mixture was briefly sonicated to redisperse the sample and was then filtered through a 0.2 μm fluoropore FG filter, and washed with NMP until the filtrate ran clear. The sample was redispersed in NMP (50 mL), and the entire procedure was repeated an additional two times. Finally, the solid was washed with methanol and dried under vacuum to afford 49 mg of black solid. A portion of this material was dialyzed (10-13kDa CO) against medical grade sterile water (Baxter) for 5 days. The 5-day dialysis entailed two daily changes of water preceded by a 60- to 90-min sonication at 80kHz. At the end of the dialysis period, all preparations were placed in sterile glass containers and lyophilized until dry.

Tour-functionalized CNOs (f-CNOs): Synthesis was performed using similar reaction conditions as previously described.[28] A 40 mg quantity was dispersed in DMF (100 mL) by sonication. To this dispersion was added firstly the 4-aminobenzoic acid (3.3 g) and subsequently isoamyl nitrite (5.36 mL) under a nitrogen atmosphere. The reaction was stirred overnight at 60 °C and subsequently allowed to cool to room temperature. The CNOs were separated from the reaction solution by centrifugation. Fresh DMF was added following removal of the supernatant. This procedure was repeatedly conducted until the supernatant solution remained colorless. This was repeated with toluene and methanol and the black solid was finally dried under reduced pressure to afford 38 mg of black solid (yield: 95%). A portion of this material was dialyzed (10–13 kDa CO) against medical grade sterile water (Baxter) for 5 days. The 5-day dialysis entailed two daily changes of water preceded by a 60- to 90-min sonication at 80kHz. At the end of the dialysis period, all preparations were placed in sterile glass containers and lyophilized until dry.

Fluoroscein-Functionalized CNTs (Fluo-CNTs): A 13 mg quantity of *f*-CNTs was dispersed in dry dimethylformamide (DMF) by sonication for 1 h. Dimethylaminopyridine (DMAP) and N-hydroxysuccinimide were added to the mixture and sonicated at minimum power for 10 min. Subsequently, 1-ethyl-3-(3-dimethylaminopropyl)carbodiimide (EDCI) was added and the dispersion was sonicated for 3 hours at low power under a N_2 atmosphere. Finally, fluorosceinamine was added and the dispersion was allowed to stir at 60 °C for 6 days under a N_2 atmosphere. The dispersion was briefly sonicated to redisperse the sample and was then filtered through a 0.2 μm fluoropore FG filter, washing with DMF until the filtrate ran clear. The sample was redispersed in DMF, and the entire procedure was repeated an additional two times. Finally, this material was dialyzed (10–13 kDa CO) against medical grade sterile water (Baxter) for 5 days. The 5-day dialysis entailed two daily changes of water preceded by a 60- to 90-min water bath sonication at 80 kHz. At the end of the dialysis period, all preparations were placed in sterile glass containers and lyophilized until dry.

Fluoroscein-Functionalized CNOs (Fluo-CNOs): An 8 mg quantity of *f*-CNOs was dispersed in dry DMF by sonication for 1 h. Dimethylaminopyridine (DMAP) and N-hydroxysuccinimide were added to the mixture sonicated at minimum power for 10 min. Subsequently, 1-Ethyl-3-(3-dimethylaminopropyl)carbodiimide (EDCI) was added and the dispersion was sonicated for 3 h at low power under a N_2 atmosphere. Finally, fluorosceinamine was added and the dispersion was allowed to stir at 60 °C for 6 days under a N_2 atmosphere. The dispersion was centrifuged at a rcf of 6870g for 60 min and the supernatant removed. The wet solid was redispersed in DMF and again separated from the supernatant by centrifugation (this was repeated an additional two times). Finally, this material was dialyzed (10-13 kDa CO) against medical grade endotoxin-free sterile water (Baxter) for 5 days. The 5-day dialysis entailed two daily changes of water preceded by a 60- to 90-min sonication at 80 kHz. At the end of the dialysis period, all preparations were placed in sterile glass containers and lyophilized until dry.

Prior to in vitro or in vivo experiments, all formulations were prepared by weighing the freeze-dried preparations into sterile glass tubes and diluting them down to the desired concentrations in sterile, endotoxin-free, phosphate buffered saline (PBS) solution. The solutions were then sonicated for 15 min at 30 kHz, 100% intensity, followed by a sonication at 80 kHz for 90–120 min.

Characterization of Carbon Nanotubes and Nano-Onions: Dynamic light scattering (DLS) and zeta potential measurements were conducted on a Malvern Zetasizer Nano ZS system (Malvern Instruments Ltd.) using a HeNe laser (633 nm). For the measurement of zeta potential the carbon nanoparticles (35 μg) were

small 2013,
DOI: 10.1002/smll.201300481

NANO MICRO small

dispersed in low ionic strength 0.01 M phosphate buffer (1.4 mL, pH 7.3) by sonicating them for 15 min at 30 kHz and then for 90 min at 80 kHz prior to measurement. The measurement was conducted at 25 °C six times and the average was calculated. For the DLS measurements the samples were prepared the same way as for the zeta potential measurements but using the sterile phosphate buffered saline (PBS) solution as solvent to replicate the sample preparation used for the in vitro and in vivo experiments. The DLS measurement was carried out repeatedly for a duration of 200 min to observe the agglomeration tendency as a function of time.

AFM: Topographic images were collected in semi-contact mode with an NTEGRA Spectra inverted configuration system (NT-MDT). Silicon tips with reflectance gold coating on the back, tip apex radius 10 nm, force constant 2 N/m and frequency 170 kHz were used (NSG01 (NT-MDT)). The data were collected with NT-MDT Nova software and analysed with WSxM SPM freeware.[57] Samples were prepared by dispersing the nanotubes in high purity DMF by sonication, spray coating them onto freshly cleaved mica substrates and drying them overnight in the oven at 100 °C. For the SWNT size distribution analysis, samples were dispersed at lower concentration in order to adequately estimate single nanoparticle size. Statistical analysis was performed on samples of >100 SWNTs. The contour length of individual SWNTs was measured using the segmented line profiling tool from WSxM SPM freeware. Statistical analysis of CNO size was performed using ImageJ.

Micro-Raman Scattering: Measurements were performed at room temperature in backscattering geometry using a NTEGRA Spectra Upright configuration system (NT-MDT) coupled with an InVia spectrometer (Renishaw) equipped with a 1024 × 256 pixels CCD camera. As excitation sources a HeNe laser (λ_{ex} 633 nm) and an Ar^+ laser (λ_{ex} 514 nm) in combination with a 1800 or 2400 lines mm^{-1} grating, respectively, were used. Measurements were taken with 10 s of exposure time. The laser spot was focused on the sample surface using a 100× long working distance objective (NA 0.7). Raman spectra were collected on numerous spots of the sample. Data were collected and analysed with Renishaw WiRE software.

TEM: Measurements of CNTs and CNOs were performed with a Hitachi Model 9500 and FEI Titan operated at 300 kV, respectively. CNO samples were prepared from dispersion followed by deposition on the copper grids. CNT samples were prepared by drop coating SWNT dispersions in DMF onto a lacey carbon coated 400 mesh copper grid.

FTIR: Spectra were measured in the solid state on a PerkinElmer FTIR Spectrometer Spectrum 100 with a universal ATR sampling accessory (diamond/ZnSe crystal). The spectra for functionalized CNOs and SWNTs were recorded at 256 scans, with a 4 cm^{-1} resolution.

UV-Vis Absorption: Spectra were recorded on a Perkin Elmer UV/Vis Spectrometer Lambda 35 after 1 cycle, with an interval of 1 nm, slit width of 2 nm and scan speed of 240 nm min^{-1}. Absorption spectroscopy was carried out on a Perkin Elmer UV-vis/NIR Lambda 1050 Absorption Photospectrometer. All spectra were recorded on supernatants after 1 cycle, with an interval of 1 nm, slit width 2 nm and scan speed of 240 nm min^{-1}. Samples were either dispersed in NMP or DMF by sonication (3–4 h) and measurements were carried out in a 1 cm quartz cell on the dispersion supernatant following centrifugation at 8000 RPM (900 × g) for 90 min (to remove aggregates and large bundles). Emission spectra were taken in a HORIBA Jobin Yvon Fluorolog-3 Spectrofluorometer equipped with a 450 xenon CV lamp after 1 cycle, with slit width of 10 nm and integration time 0.1 s.

Raman Spectroscopic Analysis of Lymph Node Tissue: Micro-Raman scattering measurements were carried out at room temperature in backscattering geometry using a NTEGRA Spectra Upright configuration (NT-MDT) coupled with an InVia spectrometer (Renishaw) equipped with a 1024 × 256 pixels CCD camera. As excitation sources an Ar^+ laser (λ_{exc} 514 nm) in combination with a 2400 lines mm^{-1} grating was used. In all measurements the laser power did not exceed 5 mW. Measurements were taken with 10 s of exposure time and 1 accumulation. The laser spot was focused on the sample surface using a 100× long working distance objective (NA 0.7). Spectroscopic data were collected and analysed with Renishaw WiRE software. Lymph nodes for Raman analyses were put on a cleaned silicon substrate and covered with a thin layer of fixation solution (4% paraformaldehyde).

Mice Source and Husbandry: Female C57BL/6 wild-type mice aged 8–12 weeks were obtained from Harlan Laboratories (Oxon, UK). $NLRP3^{-/-}$ mice[58] were age- and gender-matched with C57BL/6 wild-type mice for each set of experiments. Animals were maintained on a light/dark cycle with at least 12 h of light and water was provided ad libitum. All animal experiments were conducted according to the regulations of the European Union and the Irish Department of Health, and all procedures were approved by the Animal Ethics Committee (reference number 091210) at Trinity College Dublin.

Measurement of Dendritic Cell Activation: Murine bone-marrow-derived dendritic cells (BMDC) generated as previously described[59] were plated out on day 10 and primed with TLR agonists (LPS, CpG, Pam3CSK4) on day 11 for 1–2 h prior to stimulation with either alum (Brenntag Biosector, Frederikssund, Denmark) or carbon nanoparticles (*r*-CNT, *p*-CNT, *f*-CNT, *p*-CNO or *f*-CNO) at the concentrations indicated. When specified, cells were pretreated with the following chemical inhibitors prior to the addition of particulate materials: 250 nM bafilomycin (an inhibitor of lysosomal acidification) or 10μM CA-074-Me (a cathepsin B inhibitor), 50 mM KCl (for inhibition of potassium efflux). Supernatants were collected and analysed for IL-1β by ELISA (R&D Systems). IL-6 (BD Biosciences), TNF-α and IL-10 (ELISA Max set, Biolegend) were also determined by ELISA according to the manufacturers' instructions. In addition to cytokine secretion the effect of particulates on expression of costimulatory molecule expression was assessed by flow cytometry as described previously.[60] All in vitro experiments were carried out independently a minimum of 3 times.

Innate Immune Responses to Carbon Nanoparticles (Peritonitis Model): Female C57BL/6 mice (n = 3–5) aged 6–8 weeks were injected intraperitoneally with PBS vehicle, Alum (250 μg/mouse), *r*-CNTs (250 μg/mouse), *p*-CNT (250 μg/mouse), *f*-CNT (250 μg/mouse), *p*-CNO (250 μg/mouse) or *f*-CNO (250 μg/mouse). After 3 h, peritoneal lavage cells were collected and cell recruitment was analysed by flow cytometry. In order to determine the nature of the infiltrating cells, peritoneal exudate cells were stained with the following fluorescently labeled antibodies (eBiosciences, Biolegend or BD Pharmingen): CD11b-PE Cy7, Gr1-APC Cy7, F4/80 PerCP Cy5.5, Siglec F-PE, CD3-APC Cy7, CD11c APC, MHC II-PE, CD19-perCP Cy5.5, Ly6C-FITC. A Canto II (BD Biosciences) or CyAN (Dako) flow cytometer was used, and data were analysed using FlowJo software (Tree Star Inc., Ashland, OR, USA). Results were expressed as a percentage of single/live cells (Mean ± SD, $*p < 0.05$, $**p < 0.01$).

DOI: 10.1002/smll.201300481

Cell Viability of Bone-Marrow Derived Dendritic Cell Cultures: Murine bone-marrow-derived dendritic cells (BMDC) generated as previously described[59] were plated out on day 10 and incubated for 24 h on day 11 in the presence of (A) carbon nanotubes (*p*-CNT), (B) nano-onions (*p*-CNO) and (C) Alum at a range of concentrations 1–100 μg cm^{-2}. Cell viability was assessed using the LIVE/DEAD Aqua stain according to the manufacturers' instructions.

Adjuvant Properties of Carbon Nanoparticles: Female C57BL/6 mice (n = 5) were immunized intraperitoneally on days 0 and 14 with endotoxin-free Dulbecco's PBS, human serum albumin (HSA, Novozyme BioPharma UK Ltd, 50 μg/mouse) alone or HSA (50 μg/mouse) mixed with Alum (200 μg/mouse), *r*-CNTs (200 μg/mouse), *p*-CNT (200 μg/mouse), *f*-CNT (200 μg/mouse), *p*-CNO (200 μg/mouse) or *f*-CNO (200 μg/mouse). On day 21, whole blood, spleens and peritoneal lavage cells were collected. Antigen-specific serum IgG and IgG1 titers were determined by ELISA (IgG: Sigma; IgG1: antibody pairs from BD PharMingen). Mediastinal lymph node single cell suspensions were prepared and further cultured with HSA (10 μg/mL) or medium only for 72 h. Supernatants were collected and IL-10, IL-4, IL-17A and IFN-γ concentrations were determined using Max ELISA kits (Biolegend).

Confocal Microscopy Analysis: Immortalized bone marrow-derived macrophages (iBMM) from wild type C57BL/6 mice were generated using J2 transforming retroviruses (expressing Raf and Myc), as described previously.[41] iBMM or bone-marrow derived dendritic cells (5×10^5 cells mL^{-1}) were cultured on glass coverslips at 37 °C for 0–18 h with carbon nanoparticles (25 μg cm^{-2}). Cells were fixed with 2% paraformaldehyde for 20 min and stained with Alexa-Fluor 594-conjugated wheat germ agglutinin (WGA; 10 μg mL^{-1}) for 30 min. Immediately before mounting, Hoechst nuclear stain was applied to the sections for 10 min and excess was washed away. Cells were mounted onto glass slides with Dakomation mounting medium (Dako) and analysed on a Zeiss LSM 510 microscope with LSM 5 software (version 4) and Adobe Photoshop. Stably transfected mouse THP-1 expressing ASC-GFP were prepared according to a protocol previously described.[61]

Statistics: Cytokine concentrations measured by ELISA assays were subjected to ANOVA analyses. Where significant differences were found, the Dunnett's multiple comparisons post hoc test was then performed. Statistical differences in the cell numbers determined by FACS analyses were assessed using the Kruskall–Wallis test, followed by Dunn's post hoc test. Wherever applicable, omparisons between two groups were carried out using two-tailed Student's t-test. Statistical calculations were performed using the GraphPad Prism 5 package (GraphPad Software Inc., San Diego, CA, USA) and Excel. In all cases, p-values ≤0.05 were considered statistically significant ($*p < 0.05$, $**p < 0.01$ and $***p < 0.001$). Results are representative of three independent experiments, but similarly performed.

Supporting Information

Supporting Information is available from the Wiley Online Library or from the author.

Acknowledgements

This work was supported by Science Foundation Ireland (CSET pathfinder grant 48S55 and Giordani PIYRA 07/Y12/1052). This publication has emanated from research supported in part by a research grant from Science Foundation Ireland (SFI) under Grant Number 12/IA/1421. S.G. wishes to thank the L'Oreal UNESCO For Women in Science Fellowship. L.E. and A.V.C. wish to thank the U.S. National Science Foundation, grants CHE-1110967 and DMR-1205302, and the Robert A. Welch foundation #AH-0033 for generous support. We thank Dr. Jim Harris for taking mediastinal lymph node photographs and for advice on confocal microscopy analysis. Immortalized macrophages from wild-type mice were a kind gift from Douglas Golenbock, University of Massachusetts Medical School, Worcester, MA. We also thank Rebecca Coll, Dr. Sarah Doyle and Dr. Jennifer K. Dowling for technical assistance with ASC-GFP-THP-1 cells. We thank Eoghan Delany for support with the Tour-functionalization of carbon nano-onions and Nicola Pesenti for support with Raman spectroscopic measurements and statistical data analysis of carbon nanoparticle size distribution. We also would like to thank Ruza Leko for designing the ToC and cover figures.

[1] S. Iijima, *Nature* **1991**, *354*, 56.
[2] X. Zhao, R. Liu, *Environ. Int.* **2012**, *40*, 244.
[3] N. Sinha, J. T. Yeow, *IEEE Trans. Nanobiosci.* **2005**, *4*, 180.
[4] S. Y. Madani, N. Naderi, O. Dissanayake, A. Tan, A. M. Seifalian, *Int. J. Nanomed.* **2011**, *6*, 2963.
[5] Y. Liu, Y. Zhao, B. Sun, C. Chen, *Acc Chem Res* **2013**, *46*, 702.
[6] S. K. Smart, A. I. Cassady, G. Q. Lu, D. J. Martin, *Carbon* **2006**, *44*, 1034.
[7] L. A. Thomson, F. C. Law, N. Rushton, J. Franks, *Biomaterials* **1991**, *12*, 37.
[8] M. Allen, F. Law, N. Rushton, *Clin. Mater.* **1994**, *17*, 1.
[9] S. Linder, W. Pinkowski, M. Aepfelbacher, *Biomaterials* **2002**, *23*, 767.
[10] T. Thurnherr, C. Brandenberger, K. Fischer, L. Diener, P. Manser, X. Maeder-Althaus, J.-P. Kaiser, H. F. Krug, B. Rothen-Rutishauser, P. Wick, *Toxicol. Lett.* **2011**, *200*, 176.
[11] M. L. Schipper, N. Nakayama-Ratchford, C. R. Davis, N. W. S. Kam, P. Chu, Z. Liu, X. M. Sun, H. J. Dai, S. S. Gambhir, *Nat. Nanotechnol.* **2008**, *3*, 2.16.
[12] D. Urgate, *Nature* **1992**, *359*, 707.
[13] M. Ghosh, S. K. Sonkar, M. Saxena, S. Sarkar, *Small* **2011**, *7*, 3170.
[14] E. L. Chng, M. Pumera, *Chemistry* **2012**, *18*, 1401.
[15] E. Del Canto, K. Flavin, D. Movia, C. Navio, C. Bittencourt, S. Giordani, *Chem. Mater.* **2011**, *23*, 67.
[16] V. E. Kagan, Y. Y. Tyurina, V. A. Tyurin, N. V. Konduru, A. I. Potapovich, A. N. Osipov, E. R. Kisin, D. Schwegler-Berry, R. Mercer, V. Castranova, A. A. Shvedova, *Toxicol. Lett.* **2006**, *165*, 88.
[17] L. G. Delogu, S. M. Stanford, E. Santelli, A. Magrini, A. Bergamaschi, K. Motamedchaboki, N. Rosato, T. Mustelin, N. Bottini, M. Bottini, *J. Nanosci. Nanotechnol.* **2010**, *10*.
[18] K. Pulskamp, S. Diabaté, H. F. Krug, *Toxicol. Lett.* **2007**, *168*, 58.
[19] F. Flavin, I. Kopf, E. Del Canto, C. Navio, C. Bittencourt, S. Giordani, *J. Mater. Chem.* **2011**, *21*, 17881.
[20] G. A. Tynan, A. McNaughton, A. Jarnicki, T. Tsuji, E. C. Lavelle, *PloS One* **2012**, *7*, e37261.

DOI: 10.1002/smll.201300481

[21] S. L. Hem, H. Hogenesch, *Exp. Rev. Vaccines* **2007**, *6*, 685.
[22] M. W. Munks, A. S. McKee, M. K. MacLeod, R. L. Powell, J. L. Degen, N. A. Reisdorph, J. W. Kappler, P. Marrack, *Blood* **2010**, *116*, 5191.
[23] K. Schroder, J. Tschopp, *Cell* **2010**, *140*, 821.
[24] E. Meunier, A. Coste, D. Olagnier, H. Authier, L. Lefèvre, C. Dardenne, J. Bernad, M. Béraud, E. Flahaut, B. Pipy, *Nanomedicine* **2012**, *8*, 987.
[25] J. Palomäki, E. Välimäki, J. Sund, M. Vippola, P. A. Clausen, K. A. Jensen, K. Savolainen, S. Matikainen, H. Alenius, *ACS Nano* **2011**, *5*, 6861.
[26] A. S. Rettenbacher, B. Elliott, J. S. Hudson, A. Amirkhanian, L. Echegoyen, *Chemistry* **2005**, *12*, 376.
[27] K. Flavin, K. Lawrence, J. Bartelmess, M. Tasior, C. Navio, C. Bittencourt, D. F. O'Shea, D. M. Guldi, S. Giordani, *ACS Nano* **2011**, *5*, 1198.
[28] K. Flavin, N. Chaur, L. Echegoyen, S. Giordani, *Org. Lett.* **2010**, *12*, 840.
[29] M. S. Strano, C. A. Dyke, M. L. Usrey, P. W. Barone, M. J. Allen, H. Shan, C. Kittrell, R. H. Hauge, J. M. Tour, R. E. Smalley, *Science* **2003**, *301*, 1519.
[30] B. Smith, K. Wepasnick, K. E. Schrote, A. R. Bertele, W. P. Ball, C. O'Melia, D. H. Fairbrother, *Environ. Sci. Technol.* **2009**, *43*, 819.
[31] A. Savina, S. Amigorena, *Immunol Rev.* **2007**, *219*, 143.
[32] D. Yang, Y. Zhao, H. Guo, Y. Li, P. Tewary, G. Xing, W. Hou, J. J. Oppenheim, N. Zhang, *ACS Nano* **2010**, *4*, 1178.
[33] K. Inoue, R. Yanagisawa, E. Koike, M. Nishikawa, H. Takano, *Free Radical Biol. Med.* **2010**, *48*, 924.
[34] A. V. Tkach, G. V. Shurin, M. R. Shurin, E. R. Kisin, A. R. Murray, S. H. Young, A. Star, B. Fadeel, V. E. Kagan, A. A. Shvedova, *ACS Nano* **2011**, *5*, 5755.
[35] J. Palomäki, P. Karisola, L. Pylkkänen, K. Savolainen, H. Alenius, *Toxicology* **2010**, *267*, 125.
[36] T. Zhang, M. Tang, L. Kong, H. Li, T. Zhang, S. Zhang, Y. Xue, Y. Pu, *J. Hazard Mater.* **2012**, *219-220*, 203.
[37] D. Crouzier, S. Follot, E. Gentilhomme, E. Flahaut, R. Arnaud, V. Dabouis, C. Castel-larin, J. C. Debouzy, *Toxicology* **2010**, *272*, 39.
[38] A. S. Yazdi, G. Guarda, N. Riteau, S. K. Drexler, A. Tardivel, I. Couillin, J. Tschopp, *Proc. Natl. Acad. Sci. USA* **2010**, *107*, 19449.
[39] H. Li, S. B. Willingham, J. P. Ting, F. Re, *J. Immunol.* **2008**, *181*, 17.
[40] T. Fernandes-Alnemri, J. Wu, J. W. Yu, P. Datta, B. Miller, W. Jankowski, S. Rosenberg, J. Zhang, E. S. Alnemri, *Cell Death Differ.* **2007**, *14*, 1590.
[41] A. Halle, V. Hornung, G. C. Petzold, C. R. Stewart, B. G. Monks, T. Reinheckel, K. A. Fitzgerald, E. Latz, K. J. Moore, D. T. Golenbock, *Nat. Immunol.* **2008**, *9*, 857.
[42] V. Hornung, F. Bauernfeind, A. Halle, E. O. Samstad, H. Kono, K. L. Rock, *Nat. Immunol.* **2008**, *9*, 847.
[43] M. Kool, T. Thomas Soullié, M. van Nimwegen, M. A. M. Willart, F. Muskens, S. Jung, H. C. Hoogsteden, H. Hammad, B. N. Lambrecht, *J. Exp. Med.* **2008**, *205*, 869.
[44] S. Calabro, M. Tortoli, B. C. Baudner, A. Pacitto, M. Cortese, D. T. O'Hagan, E. De Gregorio, A. Seubert, A. Wack, *Vaccine* **2011**, *29*, 1812.
[45] H. Sun, K. G. Pollock, J. M. Brewer, *Vaccine* **2003**, *21*, 849.
[46] A. S. McKee, M. W. Munks, P. Marrack, *Immunity* **2007**, *27*, 687.
[47] L. Yan, F. Zhao, S. Li, Z. Hu, Y. Zhao, *Nanoscale* **2011**, *3*, 362.
[48] M. V. Ivanova, C. Lamprecht, M. J. Loureiro, J. T. Huzil, M. Foldvari, *Int. J. Nanomed.* **2012**, *7*, 403.
[49] R. K. Esch, L. Han, K. K. Foarde, D. S. Ensor, *Nanotoxicology* **2010**, *4*, 73.
[50] F. A. Sharp, D. Ruane, B. Claass, E. Creagh, J. Harris, P. Malyala, M. Singh, D. T. O'Hagan, V. Pétrilli, J. Tschopp, L. A. J. O'Neill, E. C. Lavelle, *Proc. Natl. Acad. Sci. USA* **2009**, *106*, 870.
[51] L. Ding, J. Stilwell, T. Zhang, O. Elboudwarej, H. Jiang, J. P. Selegue, P. A. Cooke, J. W. Gray, F. F. Chen, *Nano Lett.* **2005**, *5*, 2448.
[52] P. Urban, J. J. Valle-Delgado, E. Moles, J. Marques, C. Diez, X. Fernandez-Busquets, *Curr. Drug Targets* **2012**, *13*, 1158.
[53] B. Zhang, C. T. Kwok, *J. Mater. Sci. Mater. Med.* **2011**, *22*, 2249.
[54] Z. Liu, S. Tabakman, K. Welsher, H. Dai, *Nano Res.* **2009**, *2*, 85.
[55] H. L. Karlsson, J. Gustafsson, P. Cronholm, L. Möller, *Toxicol. Lett.* **2009**, *188*, 112.
[56] H. Yang, C. Liu, D. Yang, H. Zhang, Z. Xi, *J. Appl. Toxicol.* **2009**, *29*, 69.
[57] I. Horcas, R. Fernández, J. M. Gómez-Rodríguez, J. Colchero, J. Gómez-Herrero, A. M. Baro, *Rev. Sci. Instrum.* **2007**, *78*, 13705.
[58] F. Martinon, V. Petrilli, A. Mayor, A. Tardivel, J. Tschopp, *Nature* **2006**, *440*, 237.
[59] M. B. Lutz, N. Kukutsch, A. L. Ogilvie, S. Rössner, F. Koch, N. Romani, G. Schuler, *J. Immunol. Methods* **1999**, *223*, 77.
[60] E. A. McNeela, A. Burke, D. R. Neill, C. Baxter, V. E. Fernandes, D. Ferreira, S. Smeaton, R. El-Rachkidy, R. M. McLoughlin, A. Mori, B. Moran, K. A. Fitzgerald, J. Tschopp, V. Pétrilli, P. W. Andrew, A. Kadioglu, E. C. Lavelle, *PLoS Pathog.* **2010**, *6*, e 1001191.
[61] S. L. Doyle, M. Campbell, E. Ozaki, R. G. Salomon, A. Mori, P. F. Kenna, G. J. Farrar, A. S. Kiang, M. M. Humphries, E. C. Lavelle, L. A. O'Neill, J. G. Hollyfield, P. Humphries, *Nat. Med.* **2012**, *18*, 791.

Received: February 14, 2013
Revised: May 9, 2013
Published online: